Combined diffuse light reflectance and electric impedance measurements for navigation aid in deep brain surgery

Johannes D. Johansson, Patric Blomstedt, Neda Haj-Hosseini, Tommy Bergenheim, Ola Eriksson and Karin Wårdell

Original Publication:

Johannes D. Johansson, Patric Blomstedt, Neda Haj-Hosseini, Tommy Bergenheim, Ola Eriksson and Karin Wårdell, Combined diffuse light reflectance and electric impedance measurements for navigation aid in deep brain surgery, 2009, Stereotactic and Functional Neurosurgery, (87), 2, 105-113.
http://dx.doi.org/10.1159/000202977

Combined diffuse light reflectance and electric impedance measurements for navigation aid in deep brain surgery

Johannes D. Johansson[1], Patric Blomstedt[2], Neda Haj-Hosseini[1], A. Tommy Bergenheim[2], Ola Eriksson[1,3] and Karin Wårdell[1]

[1]Department of Biomedical Engineering, Linköping University, Sweden

[2]Department of Neurosurgery, Norrland´s University Hospital, Umeå, Sweden

[3]Elekta instrument AB, Sweden

Running title: Light and impedance for navigation in brain

Correspondence to:

Johannes Johansson

Department of Biomedical Engineering

Linköping University

581 85 Linköping

Sweden

Email: johjo@imt.liu.se

Phone: +46-13-222464

Fax: +46-13-101902

Version 2.1, 7 Nov. 08

Keywords: Stereotactic surgery, navigation, electric impedance, light reflectance

Abstract

Aim

The aim of this study is to investigate reflected light intensity combined with impedance for navigation aid during stereotactic neurosurgery.

Methods

During creation of 21 trajectories for stereotactic implantation of deep brain stimulation electrodes in the globus pallidus internus or subthalamus (zona incerta or subthalamic nucleus), impedance at 512 kHz and reflected light intensity at 780 nm were measured continuously and simultaneously with a radio frequency electrode containing optical fibres. The signals were compared with anatomy determined from pre- and postoperative MRI and CT. The measurements were performed within minutes and signal analysis was done post-operatively.

Results

Reflected light intensity was low from cortex, lateral ventricle, caudate nucleus and putamen. It was intermediate from globus pallidus and thalamus while it was high from subcortical white matter, internal capsule and the subthalamus. The electric impedance was less consistent but generally low in the cortex, intermediate in subcortical white matter, the putamen, the globus pallidus and the thalamus and high in the internal capsule and the subthalamus.

Conclusion

Reflected light intensity and electric impedance give complementary information about passed tissue and the combination seems promising for navigation aid during stereotactic neurosurgery.

Introduction

During stereotactic procedures in the deep structures of the brain, using techniques such as deep brain stimulation (DBS) [1] or radio frequency (RF) lesioning [2], an accurate, precise and safe intracerebral navigation to the calculated target is necessary. A number of methods can be used to aid targeting during stereotactic neurosurgery. These include microelectrode recording, macrostimulation [3] and measurements of electric impedance [4].

The electric impedance magnitude for navigation aid is usually measured using a radio frequency current generator. Entrance from the internal capsule into the central grey matter structures putamen, caudate nucleus, globus pallidus or thalamus can be detected by a decrease in impedance. Exit from the same grey structures into the internal capsule or the subthalamus can be detected by an increase in impedance. Cerebrospinal fluid is a much better electric conductor than grey and white matter giving very low impedance if a ventricle is entered. The method has been in use clinically since the 1960s [5, 6].

Intracerebral measurement of optical signals may be feasible for aiding the verification of pathways during stereotactic procedures. Giller and co-workers presented a system using a probe with optical fibres for intracranial near-infrared diffuse reflectance spectroscopy during stereotactic procedures in humans [7]. With their probe configuration, the reflected light intensity could be used to differentiate between white and grey matter as white matter reflects more light than grey matter. Their analysis used the slope between 700 and 850 nm in the raw spectra but this slope has been found to be almost entirely explained by the intensity around 780 nm [8]. Our group has recently used laser Doppler perfusion monitoring (LDPM) to record local blood perfusion using a near infrared laser with a wavelength of 780 nm along the trajectories to the targets during stereotactic implantation of DBS electrodes [9]. At this wavelength we do not expect the measurement to be disturbed by varying amounts of blood haemoglobin in the tissue as the light absorption from blood is low, in contrast to wavelengths beneath 600 nm where the light absorption from blood is

very high. Diffusely reflected light intensity has also been studied by us during stereotactic neurosurgery using this LDPM system [9] and a spectroscopy system [8].

The aim of this study was to compare intracerebrally recorded diffuse reflected light intensity and electric impedance magnitude with anatomy from pre- and postoperative MRI and CT and to investigate the usefulness of the methods as navigation aid in the deep brain structures.

Material and methods

Patients

14 patients (5 women, 9 men, age 35-79, mean ± s.d. = 65 ± 12) referred for unilateral or bilateral DBS-implantation in the globus pallidus internus (GPi, trajectories G1 – G10), subthalamic nucleus (STN, trajectories S1 – S5) or zona incerta (ZI, trajectories Z1 – Z6) for the treatment of Parkinson's disease, essential tremor or dystonia were included in the study. In total 21 leads were implanted. The study was approved by the local ethics committees (D. no. M182-04) in Linköping's and Norrland's University Hospitals, Sweden. Informed consent was received from each of the patients.

System for simultaneously reflected light and electric impedance measurements

An RF lesioning electrode (tip length = 2 mm, $\varnothing_{tip}$ = 1.6 mm, total length = 191 mm, functional length = 190 mm) containing four optical fibres ($\varnothing_{core}$ = 200 μm, $\varnothing_{cladding}$ = 230 μm, numerical aperture = 0.22) was used for simultaneous measurement of electric impedance and diffusely reflected light intensity (Figure 1). The dimensions of the electrode tip were requested by the surgeons in order to be small while the electrode still retains enough stiffness not to be bent. Apart from tip dimensions, the electrode was designed similar to standard monopolar RF electrodes and adapted to the Leksell Stereotactic System® (Elekta Instrument AB, Sweden). The optical fibres were aligned along the interior side of the electrode towards the tip in a fashion identical to probes used by us in earlier studies [8, 9]. With this electrode design, the tissue directly in front of the tip is investigated by the optical methods. Two fibres directly adjacent to each other were connected to a laser Doppler perfusion

monitoring system (PeriFlux 5000, Perimed AB, Sweden, laser wavelength = 780 nm, maximum output power = 1 mW) and two other directly adjacent fibres to a spectroscopy system (AvaSpec-2048-2, Avantes BV, The Netherlands) using a white lamp (AvaLight-Hal-S, Avantes BV, The Netherlands).

Stereotactic imaging

Stereotactic imaging was performed after placement of the Leksell® stereotactic frame model G (Elekta Instrument AB, Sweden). Direct anatomical targeting [10] for the STN, GPi and ZI was performed on stereotactic MRI-studies using a 1.5 T scanner (Philips Intera, The Netherlands). Adjacent trans-axial slices of 2 mm thickness with T1-weighted sequences (TR = 25 ms, TE = 5.5 ms) were collected. Proton density weighted sequences (TR = 3100 ms, TE = 20 ms) were also collected for GPi targets [11] and T2-weighted sequences [10] (TR = 4700 ms, TE = 84 ms) for STN and ZI targets. The GPi target was visually chosen in the middle of the posterior part of the GPi just dorsal and lateral to the optic tract in the proton density weighted sequences. The target in the STN was visually chosen at the line connecting the anterior borders of the red nucleus, at the level of their maximal diameter, and approximately 1.5 mm lateral to the medial border of the STN [12]. The target in the caudal ZI was visually chosen slightly medial to the medial border of the STN, in the posterior part of the posterior third of the STN. The stereotactic images were exported to the Framelink Planning Station® (Medtronic, Minneapolis, MN, USA) for calculation of target coordinates and insertion trajectory.

Surgical procedure and measurements

During surgery the RF electrode with optical fibres was used to create tracts for DBS-electrodes along the pre-calculated trajectory. Measurements of impedance and reflected light intensity were performed continuously while the surgeon manually inserted the electrode with as even speed as possible during 20 – 180 s. The optical signals, using either the laser Doppler system (n = 3) or the diffuse reflectance spectroscopy (n = 15), were logged on personal computers. Electric impedance was measured with an RF generator (Leksell® Neuro Generator, Elekta Instrument AB, Sweden) using an alternating current of 512 kHz. This RF generator can unfortunately only transmit data to a computer during lesioning so the impedance was logged by

filming the corresponding display of the generator with a digital camera. The surgeon vocally declared start and end of electrode motion for the measurements. In 5 trajectories the electrode was moved continuously directly to the target. The surgeon stopped at 1 mm above the target in 11 trajectories and LDPM and spectroscopy was performed as part of a study on the characteristics of the target nuclei. These measurements were then also performed after moving the optical electrode the very last mm to the target. In 2 trajectories the electrode was stopped 14 mm above the target after continuous insertion and LDPM, spectroscopy and impedance measurements were performed stepwise every 2 mm down to the target. In 3 trajectories only measurements in discrete points were performed giving 5 discrete measurement sequences in total. The optical electrode was thereafter removed and replaced with the DBS electrode 3387® or 3389® (Medtronic, Minneapolis, MN, USA) for macrostimulation. The positions of the DBS electrodes were verified with post-operative CT or MRI before removal of the frame. The postoperative images displaying the electrode were fused with the preoperative investigations. The evaluation concerning the electrode's relation to surrounding structures was performed with the Framelink Planning Station.

A sampling frequency of 3 kHz with electronic smoothing at a time-constant of 0.02 s was used for the LDPM system. After each surgical procedure, spectroscopy measurements, $I_{cal}(\lambda)$, were made on a white reference tile (WS-2, Avantes BV, The Netherlands) at a fixed distance from the fibre ends. Dark measurements, I_{dark}, were also made with the lamp shuttered. A sampling frequency of 12 Hz was used for the spectroscopy system.

Presentation of reflected light intensity

The light intensity measurements were normalised with the mean light intensity in a segment of white matter, $I_{0,780,whitematter}$, in the corresponding trajectory according to Eq. 1 (Figure 3a). When the spectroscopy system was used, the band 770 – 790 nm was selected in order to be comparable with the measurements using the LDPM system, which only utilises the wavelength 780 nm.

$$I(\lambda,t)=\frac{I_0(\lambda,t)}{\left\langle I_{0,780,\text{white matter}}\right\rangle} \quad \textbf{(1)}$$

In Eq. 1, λ denotes the wavelength (nm), t the time (s), and $I_0(\lambda, t)$ the raw total light intensity when the LDPM system was used and the reference tile normalised intensity when the spectroscopy system was used according to

$$I_0(\lambda,t) = \begin{cases} I_{\text{raw}}(t) & \text{LDPM system} \\ \dfrac{I_{\text{raw}}(\lambda,t) - I_{\text{dark}}}{I_{\text{cal}}(\lambda) - I_{\text{dark}}} & \text{Spectroscopy system} \end{cases} \quad \textbf{(2).}$$

From $I(\lambda, t)$ the average light reflectance in the bands 770 -790 nm, I_{780}, and 560 - 585 nm, I_{573}, were calculated (Figure 2) for presentation as one-dimensional curves when using the spectroscopy system. I_{780}- and I_{573} are presented as functions of position instead of time assuming a constant insertion speed towards the target (Figure 3).

Comparison of reflected light intensity and electric impedance with anatomy

Relevant structures and borders between them along the trajectories were identified from respective MRI by a neurosurgeon for comparison with the measured I_{780} and Z. The identified structures were cortex on top of gyri (Cort), sulcus cortex (Sulc.), subcortical white matter (Sub w), ventricles (Vent.), the caudate nucleus (CN), the internal capsule (IC), the putamen (Put), the lamina medullaris externa (LME) between putamen and globus pallidus externus (GPe), the thalamus, the lamina medullaris interna (LMI) between GPe and GPi, ZI and the subthalamic nucleus (STN).

The optical and impedance signals captured along the respective trajectory were then matched to the anatomy (Figure 3). Local minima of I_{780} related to the cortex, sulci, the putamen, GPe, GPi, ventricles, the caudate nucleus and the thalamus were taken in segments where the corresponding structure could be seen both in the MRI along the trajectory and as a noticeable decrease in I_{780}. Values of I_{780} from the target areas ZI and STN and maximum from the internal capsule were also noted. Three

measurements (S1, S2 and Z2) were not included in this analysis due to partial technical failure leaving a total of 15 continuous measurements. The mean and standard deviation (m ± s.d.) in each structure were calculated for the selected values. For variability comparison, the average standard deviation within all white matter segments was calculated.

Local maxima of the impedance for subcortical white matter and internal capsule and local minima for ventricles and grey matter structures except targets were observed. Z was also noted for the targets GPi, STN and ZI (Figure 3b). For the borders between the structures it was observed whether a clear increase or decrease in I_{780} and Z respectively could be seen. It is not possible to see a border between subcortical white matter and IC in the MRI so here the trend from superficial to deep white matter was noted instead. The mean and standard deviation in each structure was calculated for the selected values.

Comparison between reflected light intensity and electric impedance

For comparison with impedance, the I_{780}- and I_{573}-signals from the spectrometer and LDPM system in the continuous measurements were down-sampled through averaging to 1 Hz. Trajectories Z2, S1 and S2 were once again omitted. Comparisons between I_{780} and Z as well as Z and estimated electrode position were done using linear regression. Due to the electrode's geometry, the optical fibres measure ahead (~1 mm) of the impedance measurement (Figure 1). The way the impedance was logged also introduces some uncertainty in the time synchronisation between the impedance and I_{780}. The signals were therefore also compared with time-shifts of the optical signals of –4 to 2 s in steps of 1 s in order to find the highest and lowest coefficients of determination (R^2) for positive correlation for the continuous measurements. Comparisons between I_{780} and I_{573} as well as I_{573} and Z were similarly performed for all trajectories with spectroscopy measurement. For every comparison, lower quartile, median, upper quartile and outliers of the R^2 values were calculated. Corresponding comparisons were also done for the five discrete sequences but without any time-shifts.

Changes in impedance after the electrode's insertion was stopped and it remained still were recorded in 13 continuous and 22 discrete measurements. 95 % confidence intervals for the changes in impedance were then calculated for each group using Student's *t*-test for paired samples. All calculations were performed in Matlab 7.5 (The Mathworks Inc., U.S.).

Results

Typical spectra from different structures are presented in Figure 2. Examples of typical I_{780}, I_{573} and Z along the trajectories are presented in Figure 3 and Figure 4. Changes in reflected light intensity were generally similar over the entire spectral range. Two kinds of exceptions to this were noticed. In two trajectories (S3 and Z3) I_{573} was initially much lower than I_{780} and then the signals gradually converged (Figure 4b). In the uppermost part of the cortex, a spectrum with a shape deviating from the general shape in grey and white matter (Figure 2) could be seen in 6 of the measurements. These deviating cortex spectra had a clear peak at approximately 650 nm and very low intensity above 750 nm. The correlation between I_{780} and I_{573} had a mean goodness of fit ,R^2, of 0.88 and 0.84 for the continuous and discrete measurements respectively.

Values (m ± s.d.) of I_{780} and Z in the targets and from noticeable peaks corresponding to relevant anatomical structures along the trajectories are presented in Figure 5 and Figure 6 respectively. A clear increase in both I_{780} and Z could be seen upon entrance from the cortex into subcortical white matter in all trajectories except one (Z3) were Z was high also in the cortex. In one trajectory (G7) a ventricle was passed through resulting in a distinct decrease in both I_{780} and Z and in another trajectory (Z6) a decrease in Z could be seen when a ventricle was tangentially passed. It was generally difficult to see in the MRI whether the caudate nucleus was passed through or passed tangentially but a decrease in I_{780} could be seen there in six of the 11 trajectories to the subthalamus (Table 2). It was not possible to detect a border between subcortical white matter and IC with either method. However, a gradual or distinct increase in Z could be seen as IC was approached in 13 trajectories while I_{780} remained unchanged or even decreased in one case (G3).

Entrance into the putamen or thalamus could generally be associated with a decrease in both I_{780} and Z. In one trajectory (S5) neither I_{780} nor Z decreased when passing through the thalamus though. Clear peaks in I_{780} could sometimes be seen for lamina between putamen, GPe and GPi while Z tended to remain fairly unchanged or increase with depth in that region. Due to the limited spatial resolution, it was generally difficult to discern in the MRI which of STN and ZI the electrode entered but entrance to them from the thalamus could be associated with an increase in both I_{780} and Z in five trajectories.

The correlations between I_{780} or I_{573} and Z were very variable with goodness of fits (R^2) that could be anything from very good to nonexistent (Figure 7 and Figure 8). There was a positive correlation between Z and position for all measurements, i.e. the impedance tended to increase as the electrode was moved deeper into the brain towards the target. When recorded while keeping the electrode stationary, the impedance increased after the electrode was stopped in all measurements except one where it remained stable. The increase after the continuous measurements was (m ± s.d.) 43 ± 20 Ω (n = 13, 95 % confidence interval = 33 – 57 Ω) and increase after reaching discrete points was 59 ± 21 Ω (n = 22, 95 % confidence interval = 50 – 68 Ω).

Discussion

In this study we have investigated reflected light intensity, I, and electric impedance, Z, during insertions of an RF electrode with optical fibres along trajectories towards the GPi, STN or ZI and compared the measured signals with pre- and postoperative MRI and CT. The measurements were made continuously or stepwise within a few minutes during creation of tracts for DBS electrodes.

Previous studies has shown that diffuse light reflectance can be used to discriminate between white and grey matter [7-9]. Studying I_{780} from the grey matter structures (Figure 4a and Figure 5) it seems they can be categorised into dark and light grey tissue. Cortex, putamen and the caudate nucleus appear as darker while thalamus and,

as the name implies, the globus pallidus as lighter grey matter. The subthalamus, i.e. ZI and STN, seems to be best categorised as predominately white matter. We would have expected less reflected light from STN but otherwise these results are in good agreement with a study using myelin stained sections of the region of interest [13] indicating more myelin in the ZI than the lateral part of the thalamus and the globus pallidus and even less myelin in the medial part of the thalamus, the putamen and CN. The trajectories in this study always passed through the lateral part of the thalamus so I_{780} from more medial parts of the thalamus is expected to be lower than I_{780} obtained from thalamus in this study. There is no guarantee that an optical fibre system will perceive light intensity in the same way as the human eye as illumination and detection geometry differs. However, in this case white matter reflects more light than globus pallidus, which in turn reflects more light than cortex grey. Our system thus perceives shades of grey in a fashion similar to visual inspection. For navigation aid, I_{780} should thus be capable to verify whether structures such as the thalamus, the putamen, LME, LMI, and GPi have been entered or passed through.

Reflectance methods with fibre optics, whether for LDPM or spectroscopy, measure the characteristics of a very small, localised volume. Phantom and Monte Carlo studies on a similar probe, though with a fibre separation of 100 μm, has indicated that tissue about 1 to 1.5 mm ahead of the probe is interrogated [14]. As the fibre separation is smaller in our RF electrode with optical fibres we expect a shorter look-ahead distance. The very local measurement of I_{780} is a strength as it allows a very fine spatial resolution and is undisturbed by the bright lights in the operation room except for very superficial measurements. However, a drawback with this method is that some matter, such as blood or a membrane, pushed ahead by the electrode might block the tissue of interest partially or entirely for the optical fibres and it is very important that the optical fibres are clean before each measurement in case of multiple trajectories during an operation. A low value of I_{573} compared to I_{780} as found in trajectories S3 (Figure 4b) and Z3 probably indicates a large amount of blood ahead of the optical fibres; here probably due to blood from a ruptured superficial vessel being pushed ahead of the electrode. I_{780} did not seem to be affected by blood ahead of the fibres in our measurements. The other characteristic change to the spectral shape that could be noticed was the deviating spectra in some cortex measurements

(Figure 2). We do not know what this represents but a corticotomy with electrosurgical coagulation of superficial blood vessels is always performed in this region. The low amount of reflected light could thus possibly be due to burnt tissue, though this needs to be investigated further. Apart from the deviating cortex spectra, the ventricle spectrum, and the possible presence of blood ahead of the fibres the light intensity changes in a similar way over the entire spectral range used. Thus, for discrimination between grey and white matter, less complicated optical systems emitting and measuring light at 780 nm may be sufficient. On the other hand, the optical fibres can also be used for more advanced methods, such as laser Doppler perfusion monitoring [9], that could provide more information than just the tissue discrimination.

When investigating the impedance three principal groups are formed (Figure 6): low impedance tissue (cortex and ventricle), medium impedance tissue (subcortical white, putamen/globus pallidus, CN and thalamus) and high impedance tissue (IC and subthalamus). The correlation between impedance and I_{780} was very variable. This is in agreement with studies by other researchers showing that white matter sometimes has lower impedance than grey [5, 15, 16]. However, there is often a very distinct elevated level of impedance a bit more than halfway to the targets that seems to correspond to the internal capsule. A higher impedance in the internal capsule and corona radiata compared to surrounding white matter has also been reported [5, 17]. A possible explanation may be that the measured electric impedance beneath the cortex may be reflecting the orientation of the axons compared to the electrode tip [18]. The projection of the electrode tip surface is much larger viewed from the side (3.1 mm^2) than from below (1.2 mm^2, Figure 1) so axons oriented orthogonal to the trajectory are expected to give a lower impedance than axons with the same electric conductivity oriented parallel to the trajectory. There was a positive correlation between impedance and depth for both the continuous and the discrete measurements. This might be due to a generally lower electric conductivity in the deeper structures and/or a more parallel orientation between axons and trajectory deeper in the brain. It should not be ruled out that something with the measurement itself might affect the impedance though. While reflected light intensity seems superior to electric impedance in regard of distinguishing grey and white matter the impedance might potentially be able to detect fibre tracts that do not produce any changes in reflected

light intensity when entered. This would be worth further study using e.g. diffusion tensor MRI. For navigation aid, the electric impedance seems capable of verifying passage through CSF and white matter tracts such as the IC. The results are less conclusive than for the reflected light intensity though.

A complicating factor is that the brain is very soft and gyri may deform as the electrode is inserted. The tissue explored by the reflected light intensity is on average slightly ahead of that explored by the impedance measurement. The impedance measurement is thus expected to lag a little after the light reflectance measurement and this may be variable within a trajectory due to both the deformation of the brain and difficulty to keep a constant insertion speed manually. Such a deformation may add to the poor correlation between I_{780} and Z. Deformation and potential deviations from a constant insertion speed makes a truly objective comparison with MRI impossible, which is the major weakness of this study. Making the measurements in discrete positions alleviates these problems but at a great loss of spatial resolution and/or speed as the procedure will be more time-consuming if more measurement points are used. Also, the electric impedance rises when the electrode is still, so impedance measurements in nearby points are likely to disturb each other. An electric or mechanical drive for the RF electrode insertion could be used to improve the anatomical comparison without sacrificing spatial resolution.

In conclusion reflected light intensity in combination with impedance seems promising for navigation aid during stereotactic neurosurgery. Of these, the impedance seems best for detection of nearby CSF or large white fibre tracts such as IC while reflected light intensity seems to give best differentiation between white and grey matter of different shades. The methods are thus complementary and it would be of great interest to study reflected light intensity further in order to obtain sufficient data and experience for general clinical application.

Acknowledgements

The authors wish to express their sincere gratitude to Professor Marwan Hariz at Institute of Neurology, Queen Square, University College London and Norrland´s University Hospital for valuable scientific discussion and to the neurosurgery staff

and to the staff of the radiological unit at Norrland´s University Hospital for providing us with MR images. Our gratitude is also to be expressed to Carina Fors, M.Sc. and to research engineers Per Sveider and Håkan Rohman, Dept. of Biomedical Engineering at Linköping University for skilful Labview programming and probe construction respectively. The study was supported by the Swedish Governmental Agency for Innovation Systems (Vinnova), the Swedish Foundation for Strategic Research (SSF) and the Swedish Research Council (VR).

References

1 Benabid AL 2003 Deep brain stimulation for Parkinson's disease Current Opinion in Neurobiology 13 696-706

2 Laitinen LV, Bergenheim AT, and Hariz MI 1992 Leksell's posteroventral pallidotomy in the treatment of Parkinson's disease J Neurosurg 76 53-61

3 Gross RE, Krack P, Rodriguez-Oroz MC, Rezai AR, and Benabid A-L 2006 Electrophysiological mapping for the implantation of deep brain stimulators for Parkinson's disease and tremor Mov Disord 21 Suppl. 14 S259-S83

4 Hobza V, Jakubec J, Nemeckova J, Nemecek S, and Sercl M 1995 Impedance monitoring in the stereotactic localization of intracranial structures Sb Ved Pr Lek Fak Karlovy Univerzity Hradci Kralove 38 33-46

5 Laitinen L, Johansson GG, and Sipponen P 1966 Impedance and phase angle as a locating method in human stereotaxic surgery J Neurosurg 25 628-33

6 Zrino L and Hariz MI 2008 Impedance recording in functional neurosurgery Textbook of stereotactic and functional neurosurgery ed Tasker R (Berlin: Springer Verlag)

7 Giller CA, Johns M, and Liu HL 2000 Use of an intracranial near-infrared probe for localization during stereotactic surgery for movement disorders J Neurosurg 93 498-505

8 Antonsson J, Eriksson O, Blomstedt P, Bergenheim AT, M IH, Richter J, Zsigmond P, and Wårdell K 2008 Diffuse reflectance spectroscopy measurements for tissue-type discrimination during deep brain stimulation J Neural Eng 5 185-90

9 Wårdell K, Blomstedt P, Richter J, Antonsson J, Eriksson O, Zsigmond P, Bergenheim AT, and Hariz MI 2007 Intracerebral microvascular measurements during deep brain stimulation implantation using laser Doppler perfusion monitoring Stereotact Funct Neurosurg 85 279-86

10 Hariz MI, Krack P, Melvill R, Jorgensen JV, Hamel W, Hirabayashi H, Lenders M, Wesslen N, Tengvar M, and Yousry TA 2003 A quick and universal method for stereotactic visualization of the subthalamic nucleus before and after implantation of deep brain stimulation electrodes Stereotact Funct Neurosurg 80 96-101

11 Hirabayashi H, Hariz MI, and Fagerlund M 1998 Comparison between stereotactic CT and MRI coordinates of pallidal and thalamic targets using the Laitinen noninvasive stereoadapter Stereotact Funct Neurosurg 71 117-30
12 Bejjani BP, Dormont D, Pidoux B, Yelnik J, Damier P, Arnulf I, Bonnet AM, Marsault C, Agid Y, Philippon J, and Cornu P 2000 Bilateral subthalamic stimulation for Parkinson's disease by using three-dimensional stereotactic magnetic resonance imaging and electrophysiological guidance J Neurosurg 92 615-25
13 Gallay MN, Jeanmonod D, Liu J, and Morel A 2008 Human pallidothalamic and cerebellothalamic tracts: anatomical basis for functional stereotactic neurosurgery Brain Struct Funct
14 Giller CA, Liu HL, Gurnani P, Victor S, Yasdani U, and German DC 2003 Validation of a near-infrared probe for detection of thin intracranial white matter structures J Neurosurg 98 1299-306
15 Limonadi FM, Roberts DW, Darcey TM, Holtzheimer PE, 3rd, and Ip JT 1999 Utilization of impedance measurements in pallidotomy using a monopolar electrode Stereotact Funct Neurosurg 72 3-21
16 Rajshekhar V 1992 Continuous impedance monitoring during CT-guided stereotactic surgery: relative value in cystic and solid lesions Br J Neurosurg 6 439-44
17 Bullard DE 1989 Intraoperative impedance monitoring during CT-guided stereotactic biopsies Stereotact Funct Neurosurg 52 1-17
18 Zrinzo L and Hariz MI 2008 Impedance recording in functional neurosurgery Textbook of stereotactic and functional neurosurgery ed Gildenberg P L, Lozano A M, and Tasker R (Berlin: Springer Verlag)

Legend to figures

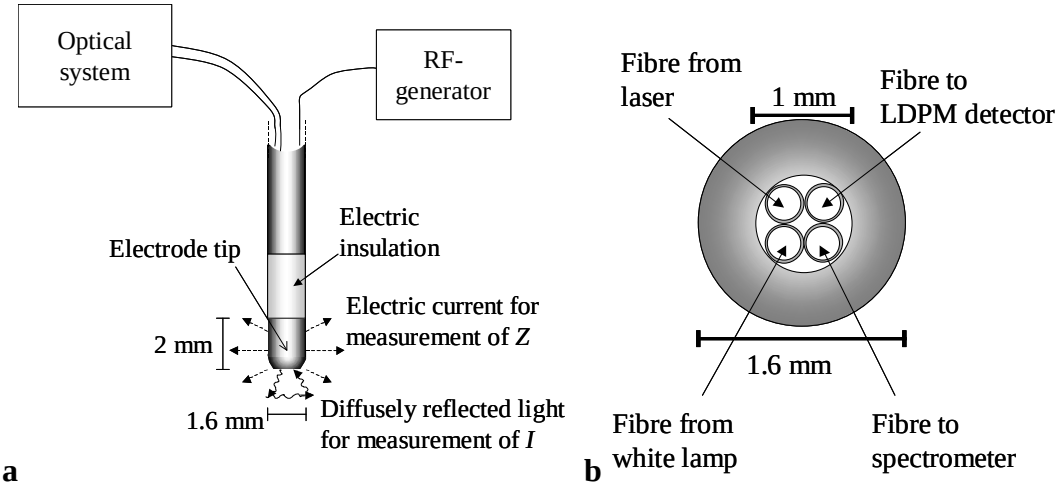

Figure 1: RF electrode with optical fibres for measurement of electric impedance and diffuse light reflectance. a: side view. b: front view.

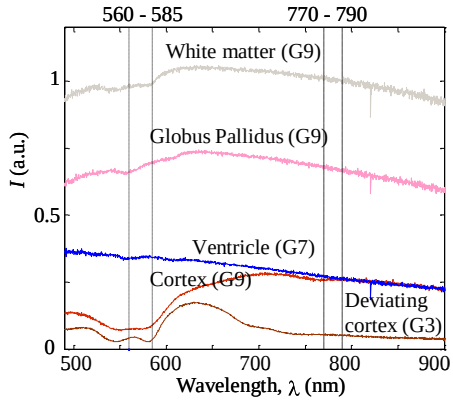

Figure 2: Typical reflection spectrums from cortex grey, GPi and subcortical white matter (G9), deviating spectrum seen in the cortex (G3) in 6 of the measurements and spectrum from the lateral ventricle (G7). Wavelength bands used for calculation of I_{573} and I_{780} are marked with vertical lines. Beneath 600 nm a decrease that corresponds to absorption due to blood can be seen. All light intensities are normalised with the mean intensity around 780 nm from a continuous segment of white matter in the corresponding trajectory.

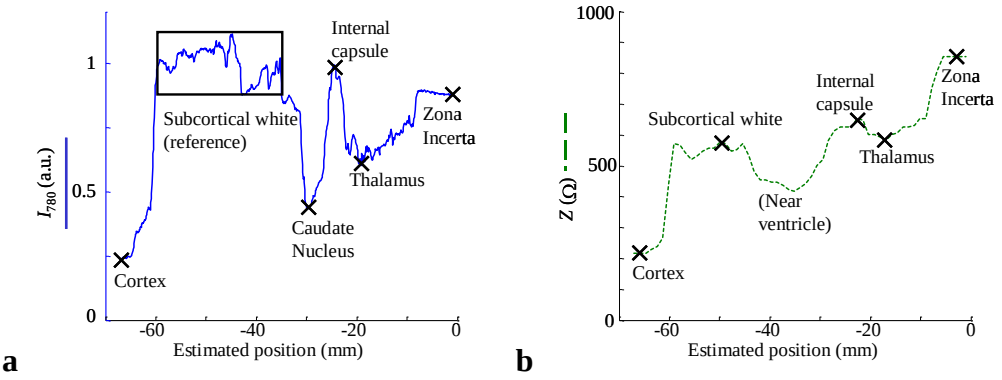

Figure 3 a: Example of I_{780} in a trajectory towards ZI (Z6). The mean intensity from subcortical white was used for normalization of all light intensities in the corresponding measurement. The crosses mark selected points for the minimal I_{780} from structures clearly visible in MRI. b: Z in the same trajectory with selected measurement spots. Local maxima of I_{780} and Z from white matter structures and local minima from grey matter structures were selected. For the targets, the values when the electrode was stopped were selected instead.

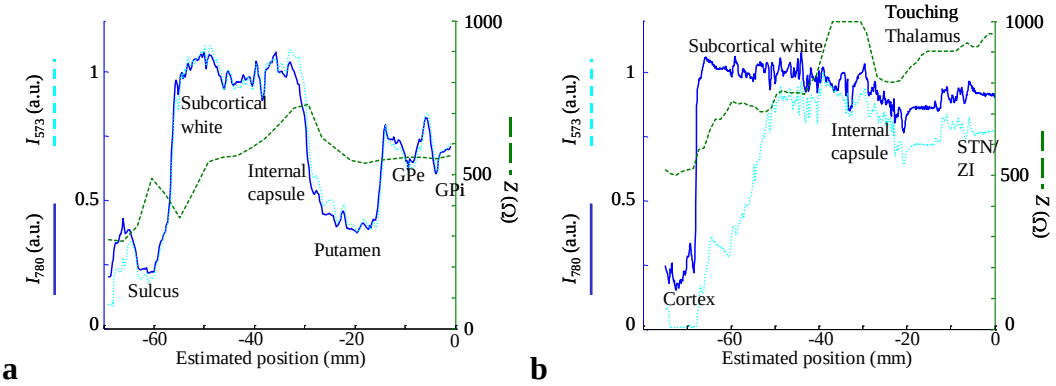

Figure 4 a: Example of I_{780}, I_{573} and impedance (Z) in a trajectory towards GPi (G10). I_{780} and I_{573} are usually changing in the same way. b: Example of I_{780}, I_{573} and impedance during electrode insertion along a trajectory towards STN (S3). In this measurement I_{573} is initially lower than I_{780}.

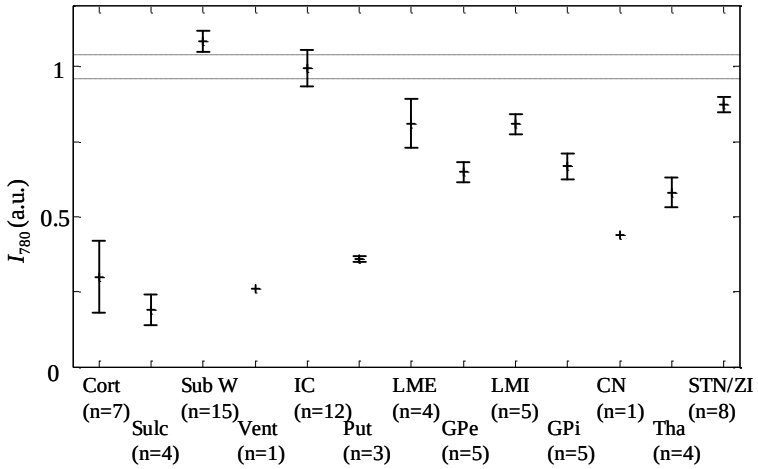

Figure 5: Reflected light intensity, I_{780}, from different structures (m ± s.d.). Intensity readings with great uncertainty about structure or where the structure was tangentially or very briefly passed were not included. Average standard deviation range within the white matter segments is marked with dotted lines. Intensities for subcortical white matter (Sub W), internal capsule (IC), LME and LMI were taken from local maxima and intensities for the ventricle and grey matter structures (Cort, Put, GPe, GPi, CN) except targets STN and ZI were taken from local minima. The intensity at the end of the measurement was taken for the targets STN and ZI.

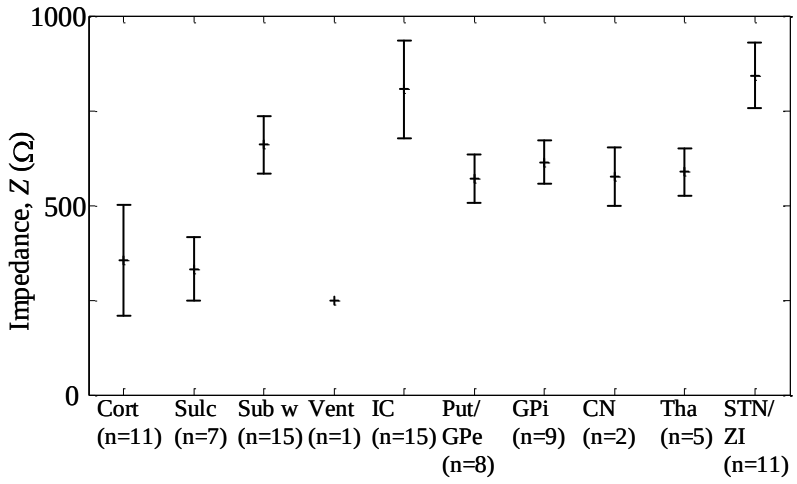

Figure 6: Impedance, *Z*, from different structures (m ± s.d.). *Z* for subcortical white matter and internal capsule were taken from local maxima and *Z* for the ventricle and grey matter structures except targets were taken from local minima. *Z* when the electrode was stopped at the target was taken for GPi, STN and ZI.

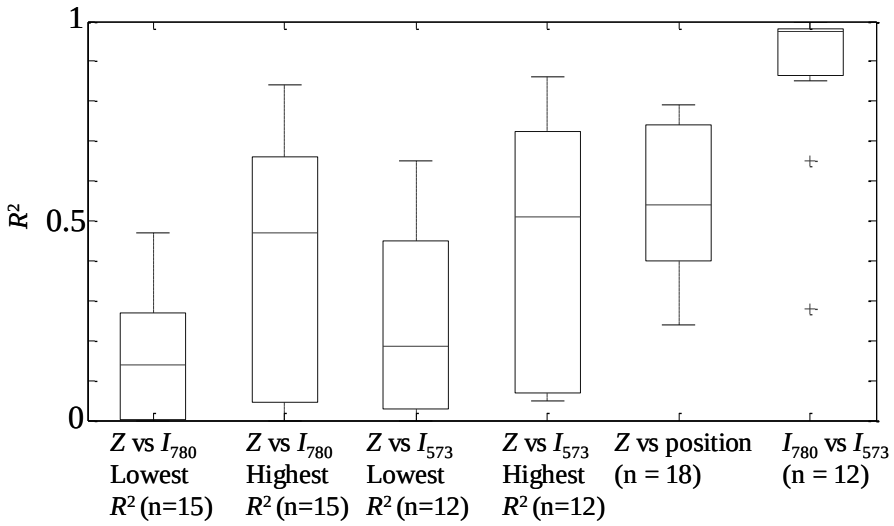

Figure 7: Boxplots of lowest and highest R^2 values for correlation between time-shifted Z and I_{780} or I_{573}, R^2 values for correlation between Z and estimated position and for correlation between I_{780} and I_{573} in the continuous measurements. Negative correlation was approximated with a R^2 value of 0. The boxes show lower quartile, median and upper quartile values while the whiskers show the minimal and maximal results. Crosses show outliers (S3 and Z3) corresponding to an initially low I_{573} compared to I_{780}.

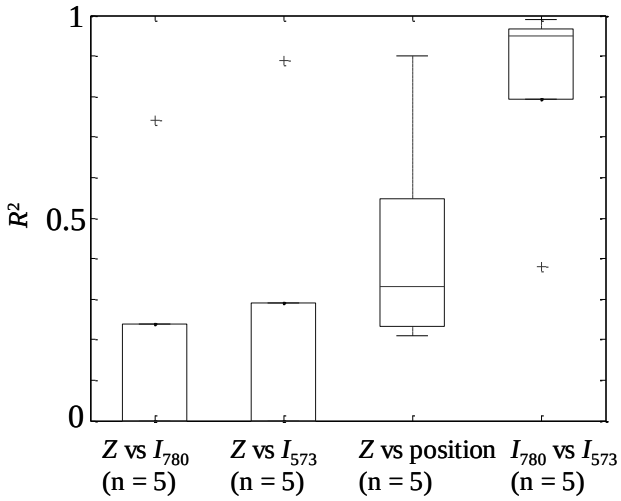

Figure 8: Boxplots of R^2 values for correlation Z and I_{780} or I_{573} and R^2 values for correlation between Z and estimated position and for correlation between I_{780} and I_{573} in the discrete measurements. The outlier for I_{780} and I_{573} corresponds to a sequence with little change in reflected light intensity.